J Mater Sci (2008) 43:4714–4728
DOI 10.1007/s10853-007-2354-7

REACTIVITY OF SOLIDS

Metal oxide composites and structures for ultra-high temperature solar thermochemical cycles

James E. Miller · Mark D. Allendorf · Richard B. Diver · Lindsey R. Evans · Nathan P. Siegel · John N. Stuecker

Received: 2 October 2007 / Accepted: 27 November 2007 / Published online: 30 April 2008

Abstract Conceptually, thermochemical cycles are heat engines that drive endothermic chemical reactions, e.g., splitting water into hydrogen and oxygen. The two-step metal oxide cycles (typically ferrite-based) are particularly attractive since they are relatively simple, use non-corrosive materials, and involve gas–solid reactions requiring no difficult separations. Additionally, they are potentially the most efficient renewable-energy driven processes for hydrogen production. We are developing a novel concentrating solar power (CSP) driven metal-oxide-based heat engine, the CR5, at the heart of which are rings of a reactive solid that are thermally and chemically cycled to produce oxygen and hydrogen from water in separate and isolated steps. The monolithic ring structures must have high geometric surface area for gas–solid contact and for adsorption of incident solar radiation, and must maintain structural integrity and high reactivity after extensive thermal cycling to temperatures of at least 1,400 °C. We have demonstrated through laboratory and on-sun testing that cobalt ferrite/zirconia mixtures fabricated into monolithic structures suitable for the CR5 are mechanically robust and maintain productivity over tens of cycles. We have also demonstrated that carbon dioxide splitting (CDS) to carbon monoxide and oxygen is a thermodynamically favorable alternative to water splitting that can be conducted with both iron- and cerium-based materials.

J. E. Miller (✉) · R. B. Diver · L. R. Evans · N. P. Siegel
Sandia National Laboratories, Albuquerque, NM 87185, USA
e-mail: jemille@sandia.gov

M. D. Allendorf
Sandia National Laboratories, Livermore, CA 94551, USA

Present Address:
J. N. Stuecker
Robocasting Enterprises LLC, Albuquerque, NM 87109, USA

Introduction

Increasing awareness of global climate change and the rising cost of conventional petroleum have fueled a growing interest in renewable and sustainable energy technologies. Solar insolation is by far the largest exploitable renewable resource [1] and is technically capable of supplying all of the world energy needs utilizing only a few percent of the world's desert area. The efficient conversion of solar energy to stored chemical energy or fuels (as envisioned for the hydrogen economy) is a significant challenge. Photosynthesis is the biological route for accomplishing this conversion, but the sunlight-to-stored chemical energy efficiency is limited by the photosynthetic step to only a few percent on average [2]. On the other hand, a reasonable estimate for photovoltaic-powered water electrolysis is 7% efficiency. In this case, the primary factor limiting solar-to-chemical efficiency is the conversion of sunlight to electricity as the electrolytic system efficiency can be up to 73% [3].

Avoiding the solar to electric conversion altogether is a potentially attractive avenue for improving the efficiency. However, thermolysis of water is not thermodynamically favorable even at an impractically high temperature of 3,000 °C. Furthermore, if direct dissociation of water were to be accomplished, it would remain to perform a difficult high-temperature quench and H_2/O_2 separation. The elegant work-around for these problems is to couple two or more chemical reactions that sum to water splitting, and then perform these reactions in a cyclic manner, recycling

all the reactants and products other than H_2O, H_2, and O_2. Although hundreds of multi-step cycles have been proposed, only a small number of those considered are judged to be practicable [4].

Conceptually, thermochemical cycles are heat engines that drive endothermic chemical reactions. The basic thermodynamic principles are described elsewhere [5]. As a caution, note that much of the thermodynamics was initially derived in the context of nuclear hydrogen production and thus some of the conclusions are based on assuming the upper temperature limit must be <1,100 °C. Concentrating solar power (CSP) provides efficient utilization of solar energy and access to temperatures in excess of 1,500 °C, and thus allows the consideration of two-step metal oxide based cycles. An example of such a thermochemical cycle based on a hypothetical metal oxide working material (MO_x) is shown below.

$$MO_x \rightarrow MO_{(x-1)} + {}^1/_2O_2$$

$$MO_{(x-1)} + H_2O \rightarrow MO_x + H_2$$

$$H_2O \rightarrow H_2 + {}^1/_2O_2$$

From a design standpoint, the relatively simple two-step metal oxide cycles are particularly attractive as they involve only gas–solid reactions. Additionally, the two reactions comprising the cycle can be temporally or spatially separated from one another, and thus no difficult gas phase separations are required, provided that additional gaseous species, e.g., an inert sweep gas to drive the equilibrium, are not required, and that the metal oxide is high melting and non-volatile.

The prototypical metal oxide thermochemical cycle is the iron oxide cycle, first promoted by Nakamura [6].

$$Fe_3O_4 \rightarrow 3FeO + {}^1/_2O_2$$

$$3FeO + H_2O \rightarrow Fe_3O_4 + H_2$$

$$H_2O \rightarrow H_2 + {}^1/_2O_2$$

The thermodynamics (temperature requirements) and materials properties (melting points in particular) for the basic ferrite cycle make implementation of the cycle as written impractical if not impossible. Thus, much research has focused on modifying the properties of the ferrite through metal substitution, with significant success [7–14]. An important advance was the recent discovery by Kodama that combining the ferrites or mixed-metal ferrites with an "inert" support, e.g., zirconia or yttria-stabilized zirconia (YSZ), produces a material that gives repeatable behavior over numerous cycles without extensive processing (e.g., grinding to a fine powder) being required between each sequence [7]. This breakthrough allowed for the first time contemplation of new and practical systems for implementing thermochemical water splitting.

The counter-rotating-ring receiver/reactor/recuperator

Conceptual design

For metal-oxide systems the oxygen-producing thermal reduction (TR) step is highly endothermic and typically requires temperatures of over 1,600 K. The hydrogen-producing water oxidation (WO) or hydrolysis step is slightly exothermic and is generally thermodynamically favorable (ΔG is negative) at ambient temperature to about 1,200 K. It is necessary therefore to cycle the temperature of the oxide as well as the gaseous environment. The required temperature cycling introduces large efficiency losses into the system unless the heat is recuperated between cycles. For example, simple thermodynamic analyses show that for the basic Fe_3O_4/FeO system operating at temperatures of 2,300 K (TR) and 600 K (WO), the maximum thermal to chemical efficiency that can be obtained is only 36%. However if heat is recovered from the cooling step and applied to reheat the working oxide, the maximum possible efficiency is increased to 76% [15].

Realizing that thermal management (recuperation of heat) is essential, we are currently developing a novel, solar-driven metal-oxide-based heat engine, the Counter-Rotating-Ring Receiver/Reactor/Recuperator, or CR5, for producing hydrogen and oxygen from water [15–18]. Briefly, the key feature of the CR5 is stack of counter-rotating rings or disks that are outfitted with fins around the circumference that are constructed of a reactive metal oxide. As the rings rotate, the reactive material passes from a solar-irradiated high-temperature TR receiver/reactor to a relatively low-temperature hydrolysis reactor where the reactant material undergoes a WO reaction, and then back again (Fig. 1). That is, the fins are cyclically heated and reduced, and then cooled and oxidized. Each ring rotates in the opposite direction to its neighbor at a rotational speed on the order of one RPM or less. The thickness of the reactant fins is a fraction of the thickness of the rings to permit solar flux to penetrate in depth and allow for water and products to be transported to and from the reactant material of the fins. Solar flux illuminates the fins on the stack of rings on edge along nominally 1/4 of the perimeter. The WO reactor is on the opposite 1/4 of the perimeter. The remaining half (two 1/4 sections between) is adiabatic and is reserved for counter-current recuperation of heat. In these two sections, thermal radiation transfers sensible heat from the hot solid-state reactant leaving the TR section to preheat the oxidized reactant entering from the WO section. Equal pressures are maintained in the two reactor sections to minimize cross flow through the recuperator sections.

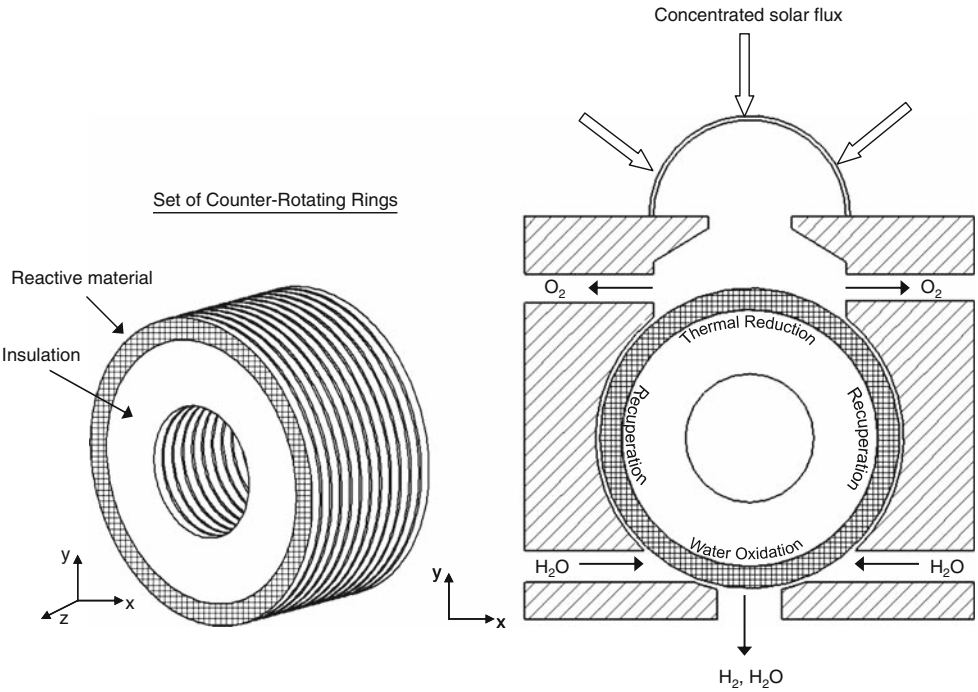

Fig. 1 Schematic of the Counter-Rotating-Ring Receiver/Reactor/Recuperator (CR5)

Materials requirements

The CR5 design, although quite attractive for achieving high efficiency (calculations suggest 30% thermal efficiency is possible [15]), and continuous operation, is very demanding of the reactive oxide working material. From a chemistry point of view it is essential for the Gibbs free energy of reaction (ΔG) to be negative (i.e., the reaction to be thermodynamically favorable) for both the TR and WO steps at reasonable temperatures and for the high-temperature TR step to couple well with the energy source. For CSP, this implies a temperature for TR $>$ 1,000 °C. It is possible of course to compensate for unfavorable thermodynamics by providing additional work to the system, although the overall system efficiency will suffer. For example, the reactions can be driven forward by keeping the system from reaching equilibrium with an inert sweep gas (this will require a separation to be performed) or similarly by operating at reduced pressure. A closely related requirement is that the solid working material must not melt or volatilize under either reaction condition. Furthermore, the chemistry must be repeatable over thousands, if not millions, of cycles. This implies that there must not be any thermodynamically or kinetically stable phases that can potentially trap the material in an inactive form. In addition to these basic chemical requirements it is desirable for the overall reaction kinetics to be as rapid as possible. That is, the surface reaction and transport of ions in and out of the bulk oxide to the reacting surface should be as rapid as possible.

From an engineering design standpoint, the working oxide must be amenable to fabrication into physical forms that can be integrated into the engine design concept. High volumetric and mass utilization of the working material is important to achieve high efficiency, even with the recuperation aspect of the CR5 design. Thus, the physical form of the metal oxide should have a high surface to volume ratio. The physical form should also be relatively open to allow gaseous transport and light penetration for direct solar heating. The parts must not physically or chemically degrade over thousands or millions of cycles and thus should be resistant to thermal shocking, have relatively small volumetric changes with changes in temperature or phase, and should be compatible with the other materials of construction.

The next several sections of this paper address these design requirements and describes our efforts to develop a working material with which to implement the CR5 design.

Thermodynamics of metal oxide thermochemical cycles

Basic thermodynamic considerations

The basic premise of thermochemical water splitting cycles is that the desired water splitting reaction ($H_2O \rightarrow H_2 + \frac{1}{2} O_2$) can be accomplished with a thermal energy input under more reasonable conditions than direct thermolysis by replacing the single reaction that has unfavorable thermodynamics at most conditions with two or more reactions

that sum to water splitting and that each have favorable thermodynamics. In other words for each step in the thermochemical cycle the Gibbs free energy change (ΔG°) of the reaction should be negative in a temperature range far below that of water thermolysis. Restating this for the hypothetical two-step metal oxide cycle shown, ΔG_1° and ΔG_2° should be <0 at 298 K < T << T_{WS}, where T_{WS} is the temperature of water thermolysis (>2,500 K for a significant degree of dissociation)

$$MO_x \rightarrow MO_{(x-1)} + {}^1/_2O_2 \qquad \Delta G_1^\circ = \Delta H_1^\circ - T\Delta S_1^\circ$$

$$MO_{(x-1)} + H_2O \rightarrow MO_x + H_2 \qquad \Delta G_2^\circ = \Delta H_2^\circ - T\Delta S_2^\circ$$

$$H_2O \rightarrow H_2 + {}^1/_2O_2 \qquad \Delta G_{WS}^\circ = \Delta H_{WS}^\circ - T\Delta S_{WS}^\circ$$

As shown, if the reactions sum to the water splitting reaction, at any given temperature the Gibbs free energy change (ΔG°) of the reactions must also sum to ΔG° of water splitting at that temperature. This fact combined with the temperature requirement and the fact that ΔG_{WS}° is always positive at temperatures of interest and has a negative slope with temperature (see Fig. 2), has several implications. At any temperature where ΔG_1° is negative, ΔG_2° must be a positive number equal to $\Delta G_{WS}^\circ - \Delta G_1^\circ$. Conversely, at any temperature where ΔG_2° is negative, ΔG_1° must be a positive number equal to $\Delta G_{WS}^\circ - \Delta G_2^\circ$. In other words, ΔG_1° and ΔG_2° must have opposite slopes (one positive, one negative) as a function of temperature (refer to curves A and B in Fig. 2), or one reaction must have a positive entropy change and the other negative (for this discussion we make the reasonable assumption that ΔH° and ΔS° of each reaction are relatively constant over the temperature range). From a more practical standpoint, this translates into a general requirement for the two steps to be carried out at different temperatures.

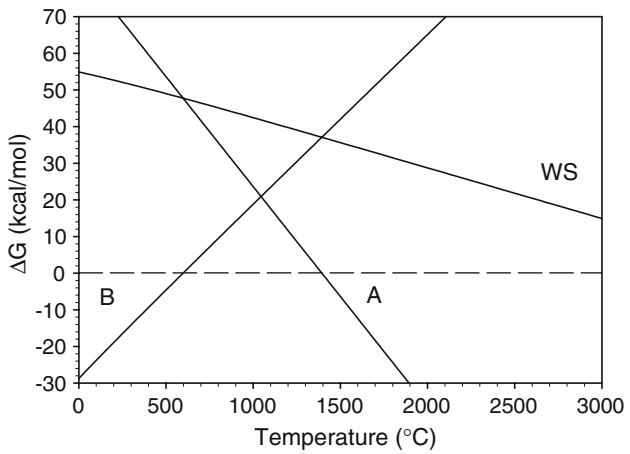

Fig. 2 Plot of the thermodynamics of the water splitting reaction (WS, $H_2O \rightarrow H_2 + ½\ O_2$) and a hypothetical two step thermochemical cycle (A and B) illustrating the relationship between the three

Going further, to meet all the constraints, ΔG° for the higher temperature reaction must have a negative slope (a positive ΔS°) and must at some point cross the ΔG_{WS}° curve (as shown for curve A). To achieve this, the high-temperature reaction must be more endothermic than WS ($\Delta H_A^\circ > \Delta H_{WS}^\circ$) and must have a slope that is more negative than that of WS ($\Delta S_A^\circ > \Delta S_{WS}^\circ$). The low temperature step will be mildly exothermic ($\Delta H_B^\circ = \Delta H_{WS}^\circ - \Delta H_A^\circ$) and have a shallower slope ($\Delta S_B^\circ = \Delta S_{WS}^\circ - \Delta S_A^\circ$). It is generally true that metal oxide reduction is endothermic, and thus the high-temperature step (curve A) corresponds to TR, and the low temperature step (curve B) to WO. Ideally ΔS° of TR will be large as this has the effect of bringing the favorable temperature ranges for the two reactions (TR and WO, curves A and B) closer together and drives the ΔG° more negative with smaller temperature changes.

Basic ferrite thermodynamics

As previously described, the iron oxide or ferrite cycle is the prototypical metal oxide thermochemical cycle. The basic thermodynamics of the ferrite cycle are illustrated in Fig. 3. It is clear from the figure that the TR step is problematic for the basic ferrite cycle. The reduction is not thermodynamically favorable at temperatures below the melting points of the relevant phases. On the other hand the WO step appears attractive. Figure 4 presents the thermodynamics for a similar cycle based on cobalt oxide. In this case, the TR step is favorable at temperatures below that of Fe_3O_4 and below the melting point of the product. Unfortunately the corresponding WO step is not thermodynamically feasible. These

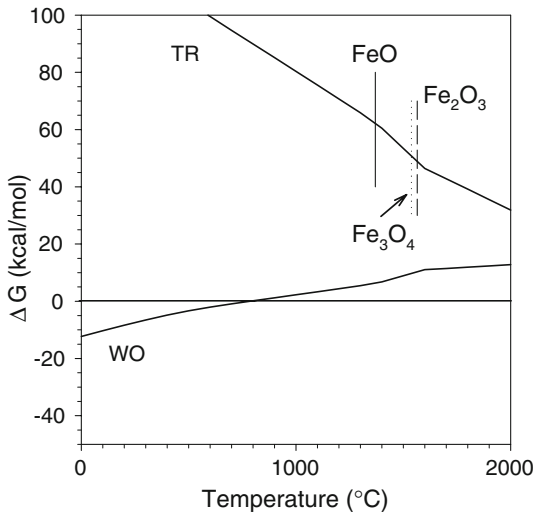

Fig. 3 Thermodynamics of thermal reduction ($2Fe_3O_4 \rightarrow 6FeO + O_2$) and water oxidation reactions ($3FeO + H_2O(g) \rightarrow Fe_3O_4 + H_2$) as calculated by HSC Chemistry 5.11 for the basic ferrite cycle. Vertical lines denote melting points of indicated iron oxide phases

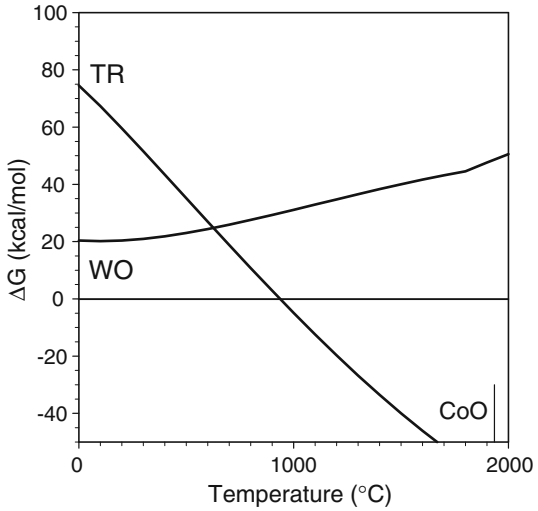

Fig. 4 Thermodynamics of thermal reduction ($2Co_3O_4 \rightarrow 6CoO + O_2$) and water oxidation reactions ($3CoO + H_2O(g) \rightarrow Co_3O_4 + H_2$) as calculated by HSC Chemistry 5.11 for a cobalt oxide cycle. Vertical line denotes melting point of CoO; Co_3O_4 decomposes to CoO prior to melting

facts have inspired researchers over the years to study mixed metal oxides as working materials for thermochemical water splitting, and success has been achieved with a number of materials including Co-, Ni-, and Mn-substituted ferrites.

Often, lowering the temperature of TR while preserving the WO activity is ascribed to a "blending" of the properties of the two (or more) metal oxides and, as here, the cobalt system is used as the illustration. The discussion should not be left here however. To elaborate, the TR of both Fe_3O_4 and Co_3O_4 involves the reduction of a metal center in a +3 oxidation state to a +2 state. Now consider that similar results for TR and WO are reported in the literature for Ni and Co-substituted ferrites. Unlike Co, however, Ni does not commonly exist in a +3 oxidation state, and furthermore the +2 state is not readily reducible. Additionally, the literature shows that Co exists almost exclusively in the +2 state in $Co_xFe_{3-x}O_4$ when $x < 1$ [19]. Thus, the positive effect cannot result from a direct "blending" of the materials, i.e., the presence of different and more easily reducible cations in the +3 valence, as the example of cobalt oxide suggests.

We have recently applied thermodynamic models to better understand the thermochemistry of mixed metal ferrites, and the effect of metal substitution on the TR process [18, 20]. Relatively simple databases such as those available in HSC Chemistry for Windows suggest that the positive effect results from limiting the amount of FeO that is formed. That is, oxides such as CoO and NiO are thermodynamically preferred over FeO. Therefore, at low levels of reduction, the reaction would be expected to proceed by the reduction of Fe(III) to Fe(II) and the "expulsion" of the substituted oxide (e.g., CoO) and O_2.

$$CoFe_2O_4 \rightarrow Co_{1-x}Fe_2O_{4-(4x/3)} + xCoO + (x/6)O_2 \ (0 \leq x \leq 1)$$

According to this simple model, Co-free Fe_3O_4 would be formed just prior to the evolution of any FeO from TR. In other words, the reduction could be thought of as occurring in two stages, reduction of Fe(III) to Fe(II) accompanied by CoO formation and ultimately Fe_3O_4 formation and then further reduction of Fe(III) with the formation of FeO. For a stoichiometrically substituted material, 1/3 of the theoretical maximum O_2 yield would be liberated in the first stage.

$$\text{Stage 1}: 6CoFe_2O_4 \rightarrow 4Fe_3O_4 + 6CoO + O_2$$
$$\text{Stage 2}: 4Fe_3O_4 \rightarrow 12FeO + 2O_2$$

Calculations performed with the more sophisticated FactSage database confirm the basic premise that metal substitution avoids FeO formation per se, but also indicate that as reduction proceeds solution phases (containing FeO and CoO, for example) contribute to driving the thermodynamics. Other reactions, for example dissolution of Fe into a solid ZrO_2 support, may also occur. Intuitively, the pathway for formation of solution phases is more direct than those for phase separation, and the formation of solution phases seems more consistent with reports in the literature of wustite (FeO) being observed by XRD after TR of cobalt- and nickel-substituted ferrites. However, there are also reports of the reduced phase from $NiFe_2O_4$ containing more NiO than FeO for example [13]. To summarize, thermodynamic models suggest that during TR of mixed metal ferrites, Fe(III) centers are reduced to Fe(II), as they are for TR of Fe_3O_4, but that this reduction is rendered more favorable by the second metal as they introduce alternatives to FeO formation, e.g., CoO, NiO, or solutions of these phases with FeO.

Overall, the efficacy of metal substitution for lowering the TR temperature while maintaining WO activity is well established. However, the particular metal best suited for this role is less certain. Calculations comparing the partial pressure of O_2 (degree of decomposition) as a function of temperature over AFe_2O_4 (A = Ni, Co, and Zn) were performed using FactSage to provide insight into this question [18]. Melting point was also considered. Overall, Ni best meets the criteria for ease of reduction and high melting point, having the highest O_2 pressure at all temperatures below ca. 1,800 K, and the highest melting point (1,860 K). For the conditions posed (0.2 g ferrite mixed with 0.8 g ZrO_2, 20 cm^3 total volume), the calculated partial pressure of O_2 over $NiFe_2O_4$ exceeds 0.21 atm at only 1,760 K. According to the calculation then, partial TR of this material could be carried out in an air environment without the occurrence of melting. Although the CR5 design does not require TR be performed in air, we

consider this to be an important threshold to help minimize the energy cost of pumping O_2 from the reaction chamber. The partial pressures of O_2 over $CoFe_2O_4$ and $ZnFe_2O_4$ are lower than $NiFe_2O_4$ under these conditions, but significantly better than Fe_3O_4, as expected. In these cases, however, the partial pressure of O_2 exceeds 0.21 atm at about the same temperature of melting (1,800 K).

Materials and structures for the CR5–experimental methods

Baseline composition

In initial work reported elsewhere [16] we synthesized and compared Ni-, Mn-, Ni/Mn-, and Co-doped ferrite powders with the goal of identifying a baseline material for our development efforts that gave readily reproducible results and reasonable hydrogen yields. Additionally we desired a material that was easily synthesized and that could be fabricated directly into monolithic structures. The study was limited in scope and was completed prior to our thermodynamic analysis pointing to Ni as a preferred component. A cobalt ferrite formulation $Co_{0.67}Fe_{2.33}O_4$ blended with YSZ in 1:3 weight ratio [14] was selected as the baseline material for further process development. To a great degree, the choice was based on the fact H_2 was reliably produced over this material, even though other materials at times gave higher yields.

Oxide synthesis and monolith construction

Synthesis of $Co_{0.67}Fe_{2.33}O_4$ was achieved through co-precipitation of the metals from nitrate solutions with ammonium hydroxide. After aging, the solids were filtered, washed with deionized water, dried in a vacuum over overnight at 80 °C, and then typically calcined for 2 h at 1,100 °C in air. The calcined ferrites were typically milled to reduce particle size to about an 11 μm average prior to testing. YSZ was used as received from Tosoh (3 mol% Y_2O_3, 0.63 μm average particle size, unless otherwise specified). Al_2O_3 (Sasol Puralox) and TiO_2 (Degussa P-25) were used as received. HfO_2 and Y-doped HfO_2 (10 mol% Y_2O_3) were synthesized by NH_4OH precipitation from solutions of $HfOCl_2$ and $HfOCl_2$ with $Y(NO_3)_3$ respectively, followed by filtration, washing, drying, and calcination at 1,100 °C.

Previous attempts at "reactorizing" ferrite powers have focused on the difficult task of supporting the ferrite on an inert monolithic substrate, e.g., SiC [21]. Our approach is to directly fabricate the powders into monolithic structures. This circumvents the need to consider the chemical compatibilities of the ferrite and substrate. This is quite important as prior experience has shown us that even very stable oxides such as hexaaluminates can interact with ceramic substrates at high temperatures in ways that are difficult to characterize, but nonetheless deleterious to performance [22]. Direct fabrication of ferrite into monolith also avoids problems such as thermal mismatch between substrate and powder coating, and allows for higher volumetric loading of the reactive material.

Physical mixtures of the ferrite powder with the support were fabricated directly into monolithic structures for testing using two different methods. The robocasting technique, developed at Sandia National Laboratories [23], was used to fabricate monoliths consisting of a series of rods arranged in a face-centered cubic-like geometry (Fig. 5a) that offers no line-of-sight pathways, yet provides three-dimensional interconnectivity of the void spaces [24]. Two sub-types of monoliths were cast with this technique, those designed to have dense, non-porous rods after firing at 1,425 °C (Fig. 5c), and those in which spherical polymethylmethacrylate (PMMA) pore former was added during the manufacture to produce a part that was nominally 75% void space (Fig. 5d). This addition required adjustment of feature sizes (rod diameters) to accommodate the larger particles. The second type of monolith was fabricated using the same slurry as the robocasting technique. In this case, however, the slurry with added pore former (75% targeted porosity) was simply poured into a cylindrical mold, allowed to dry at room temperature and then removed from the mold and fired at a temperature of at least 1,400 °C. The flat faces of the resulting disk were then ground on a bench grinder to expose the porosity (Fig. 5b). Typical specifications for these monoliths are given in Table 1. Monoliths containing other materials (Al_2O_3, TiO_2, HfO_2, and Y-HfO_2) were fabricated with similar dimensions to those in Table 1 using the second technique with the amounts of ferrite and "support" adjusted to maintain a constant volume ratio (1:3 $Co_{0.67}Fe_{2.33}O_4$/YSZ by weight is equivalent to about 1:2.6 by volume).

Water splitting reaction

The water splitting reaction was carried out in a typical laboratory-scale flow reactor consisting of a 2.53-cm-O.D. by 66-cm-long mullite tube situated in a high-temperature furnace. The ferrite composite disks are supported in the tube by plugs of refractory wool so that gas flow must pass through the thickness of the disk via the porous networks provided by the lattice structure or pore former. Argon and helium (ca. 60 sccm) are used to sweep the reactor during the WO and TR phases of water splitting, respectively. The different sweep gasses facilitate chemical analysis of the reactor effluent by gas chromatography using a thermal conductivity detector. The argon flow is split so that it can function either as an inert purge or be humidified by a

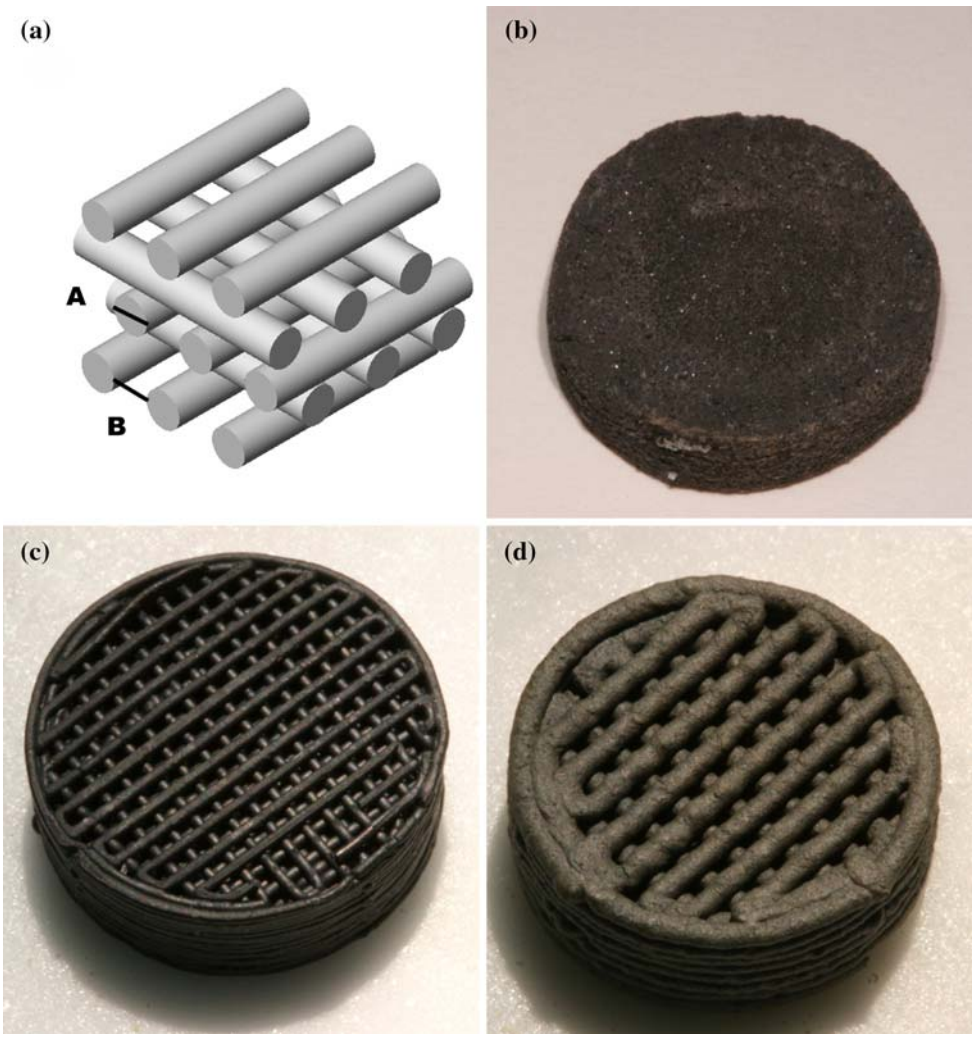

Fig. 5 Monolithic structures of 1:3 $Co_{0.67}Fe_{2.33}O_4$/YSZ. (**a**) schematic of robocast lattice structure. (**b**) Cast monolith with ground faces. (**c**) Robocast lattice with dense rods. (**d**) Robocast lattice with porous rods

Table 1 Typical specifications for $Co_{0.67}Fe_{2.33}O_4$/YSZ (1:3 by weight) monoliths

	Cast monolith	Robocast dense monolith	Robocast porous monolith
Thickness (mm)	4.1	5.1	5.4
Diameter (mm)	15.0	15.4	15.3
Rod size (mm)	N/A	0.45	0.91
Weight (g)	1.80	2.80	1.56
PMMA size (mm)	0.035 average	N/A	0.035 average

saturator operated at 80–90 °C prior to entering the reaction zone. Gas samples are collected and analyzed at 2-min intervals during WO and TR cycles. Background oxygen levels in the system are typically measured to be between 20 and 100 ppm.

The "standard operating cycle" is outlined in Table 2. Each reaction is monitored and allowed to proceed until gas evolution returns to near baseline with this method and thus it provides a measure of the maximum yield or (material utilization) that can be achieved with the monolith under the stated conditions. A limitation of the standard operating protocol is that samples can be cycled no more than one or two times each working day. Also, the long duration of each reaction step, long purge times, and slow ramp rates arising from the large thermal mass of the system are inconsistent with the CR5 design, which requires an operating speed of about 1 rpm to maintain temperature differences across the two reaction chambers. Thus, additional methods were adopted to provide some insight into the time dependence of the yields and to shorten the time required to cycle a given sample a significant number of times. Typically, the shorter cycles involved reducing the sample in Ar rather than He for a defined time period, and then exposing the sample to steam at the WO temperature for a defined time period or until H_2 evolution was complete (Table 2). In these cases, O_2 yields could not be determined. Typically, the standard procedure was performed at the beginning of a given test to establish

Table 2 Standard operating cycle for water splitting reactor

Step	Standard procedure	Alternate procedure
1	Purge with He	Purge with Ar
2-TR	Ramp to 1,400 °C	Ramp to 1,400 °C
3-TR	Hold until O_2 evolution is complete (1.5–3 h)	Hold for specified time
4	Purge with Ar	N/A
5-WO	Initiate steam flow	Initiate steam flow
6-WO	Ramp 1,400–1,100 °C	Ramp 1,400–1,100 °C
7-WO	Hold until H_2 evolution is complete (1.5–3 h)	Hold until H_2 evolution is complete (≥30 min)
8	Repeat or cool and idle overnight	Repeat or idle

a baseline, and then again on occasion throughout the run to provide an indication of any changes that have occurred as a result of cycling the sample. The sample was allowed to cool under flowing inert gas following the final WO step of a work day.

Materials and structures for the CR5: results and discussion

In this section we present our results in the context of the desired materials properties outlined in the section "Conceptual design".

Activity over numerous cycles

Kodama and co-workers established that mixing ferrite powders with ZrO_2 or YSZ powders, typically in about a 1:3 weight ratio, results in a material that can repeatedly produce H_2 over numerous cycles without extensively grinding the material between each step. We sought to expand on this finding by establishing that solid, monolithic parts fabricated from similar composites will also produce H_2 over repeated cycles. Figure 6 summarizes the results for a cast pellet of 1:3 $Co_{0.67}Fe_{2.33}O_4$/YSZ with the specifications given in Table 1. Figure 6 clearly shows that the material is active for at least 14 cycles, and that H_2 can be produced even with very short reduction times. This is a result of the fact that the rate of TR is greatest in the initial stages, as one would expect. Additionally the data shows that there is no loss in H_2 production potential with cycling for at least 8 cycles (the last standard cycle). In fact the H_2 yields in the standard cycle show some improvement with cycling. As will be seen below, this is a consistent, but not well-understood observation. For comparison purposes we also performed an experiment with a similar 1.46 g disk constructed wholly of $Co_{0.67}Fe_{2.33}O_4$. In this case, 30-min reduction cycles resulted in the production of only 0.05 cm^3 H_2/g ferrite in the first cycle and no detectable H_2 in the second cycle. The positive effect of the added zirconia support clearly carries over to monolithic parts.

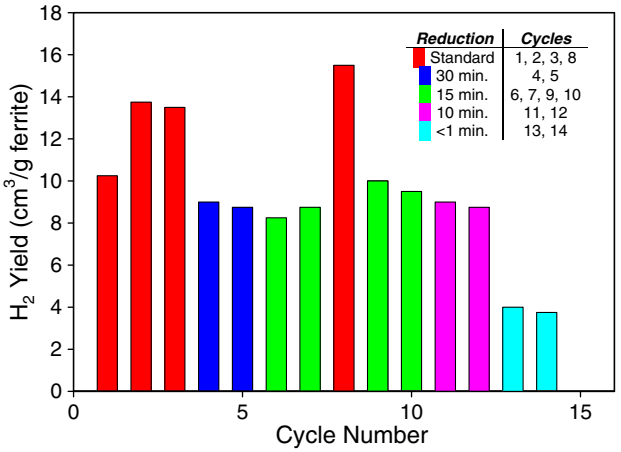

Fig. 6 Hydrogen yields for each water oxidation carried out with a cast $Co_{0.67}Fe_{2.33}O_4$/YSZ monolith

Compatibility with other supports and materials

Although constructing monoliths directly from the active ferrite/zirconia composite avoids many compatibility and reactivity issues, problems may still arise for example in places where the monoliths are joined to other reactor parts. Additionally, it is of interest to establish whether the support effect is unique to zirconia, or applies to other materials as well. Tests were carried out with disks cast from $Co_{0.67}Fe_{2.33}O_4$ mixed with either Al_2O_3 or TiO_2 in the standard 1:2.6 volume ratio. As shown in Table 3, O_2 was produced over both materials in each of the 4 TR cycles attempted. However, virtually no H_2 was produced during the corresponding WO steps. We posit that the O_2 is produced as the result of a solid-state reaction between the ferrite and support with spinels (e.g., $FeAl_2O_4$ and Fe_2TiO_4) as likely products. We were unable to confirm these reactions by powder X-ray diffraction analysis of the post-reaction monoliths (samples were characterized after crushing and after grinding to a fine powder). However, in other tests we have witnessed catastrophic reactive failure of $Co_{0.67}Fe_{2.33}O_4$/YSZ monoliths that were calcined in contact with alumina fiber board or boats at temperatures in excess of ca. 1,500 °C.

Table 3 Results of standard water splitting cycles over cast $Co_{0.67}Fe_{2.33}O_4/Al_2O_3$ and $Co_{0.67}Fe_{2.33}O_4$ /TiO_2 monoliths

Cycle number	$Co_{0.67}Fe_{2.33}O_4/Al_2O_3$		$Co_{0.67}Fe_{2.33}O_4/TiO_2$	
	O_2 produced (cm^3/g ferrite)	H_2 produced (cm^3/g ferrite)	O_2 produced (cm^3/g ferrite)	H_2 produced (cm^3/g ferrite)
1	3.8	0.00	14.9	0.15
2	2.6	0.48	12.3	0.32
3	5.6	0.48	6.5	0.05
4	6.2	0.22	4.9	0.00

In an additional set of experiments, monoliths were cast from mixtures of $Co_{0.67}Fe_{2.33}O_4$ with either HfO_2 or Y-doped HfO_2 in the standard volume ratio. The chemical properties of HfO_2 are similar to those of ZrO_2; Y-doping introduces vacancies into both ZrO_2 and HfO_2 thereby enhancing oxygen conductivity within the solid. However, unlike ZrO_2, HfO_2 is cubic with or without added Y_2O_3. The results for these monoliths are summarized in Fig. 7. Both materials produced H_2 over the 15 cycles tested, with the yields in the final standard cycles approximating those in the early cycles. The results do suggest differences in the materials however. The yields are greater and more consistent for the Y-containing sample. Also, yields over the Y-free sample appear to be somewhat independent of reduction time. Taken together this could be an indication that the reaction for the Y-free sample is limited to the outer surfaces of the material and suggests exploring the relationship between oxygen conductivity and ferrite utilization as a potentially fruitful exercise.

Integration with CR5 design concept

The robocasting method provides a route to directly produce monolithic structures with volumetric surface areas comparable to those of commercial extruded monoliths, but with the added benefits of channel to channel connectivity, no line-of-sight pathways, piece to piece consistency, and no constrictions to flow as are present in foam-like monoliths or our cast disks [24]. A computer rendering of a Robocast reactant ring segment after final machining is shown in Fig. 8 along with an early prototype cast from alumina. Small disks constructed with the lattice geometry that is integral to the current ring design were tested in our laboratory reactor to begin to establish the suitability of the robocasting technique and the lattice design for the CR5 application.

The results for the dense and porous monoliths described in Table 1 are summarized in Figs. 9 and 10, respectively. Cycles 3–8 for the porous sample (Fig. 9) were conducted in a unique fashion and will be discussed below. On the whole, the results are very encouraging. The dense sample was cycled 36 times and the porous sample was cycled 31 times, and in both cases the H_2 yield in the final standard cycle exceeded that of the earlier cycles. Additionally both samples remained mechanically sound throughout the length of the test. Under the standard conditions, the H_2 yields were greater over the dense monolith than over the porous monolith. The yields were more similar when the TR period was shortened. For shorter reduction times the reaction should be more limited to surface regions and thus this outcome indicates that the pore former did not improve ferrite utilization by providing greater surface area and access to the core of the composite rods as was hoped. This may be explained by the fact that on close inspection of the porous rods comprising the monolith the pore structure was found to have relatively

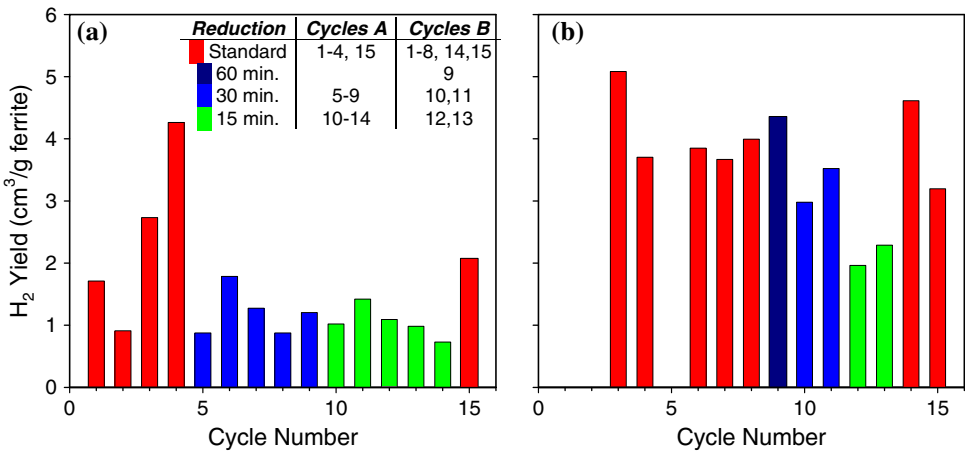

Fig. 7 Hydrogen yields for each water oxidation step carried out with cast ferrite/hafnia monoliths (**a**) $Co_{0.67}Fe_{2.33}O_4/HfO_2$ (**b**) $Co_{0.67}Fe_{2.33}O_4$/Y-doped HfO_2

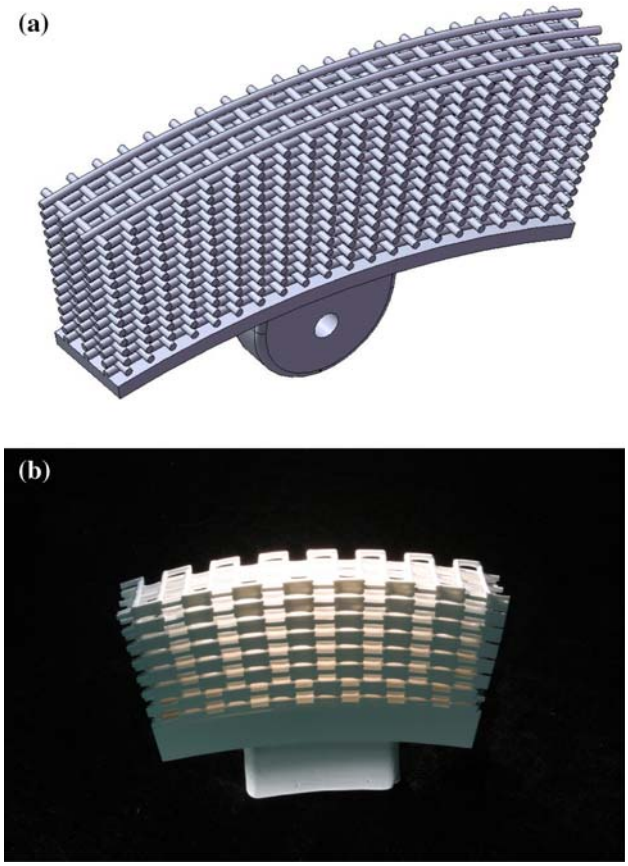

Fig. 8 Computer rendering of the Robocast reactant fin design (**a**) and an initial prototype fabricated from alumina (**b**). Each ring assembly uses 12 reactant fins. The fins are inserted into slots machined in the carrier ring, pinned in place, and secured with a zirconia adhesive

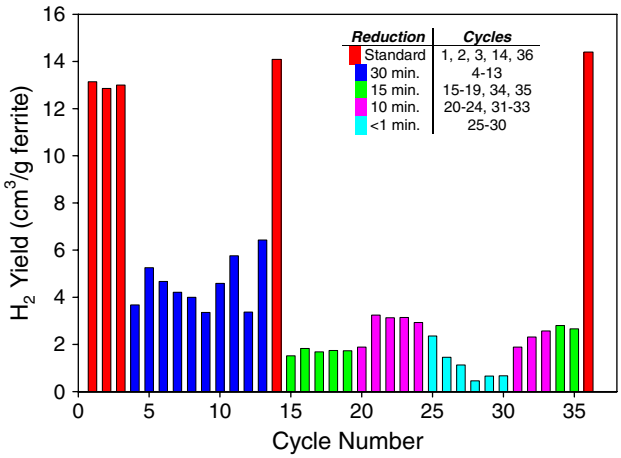

Fig. 9 Hydrogen yields for each water oxidation step carried out over a dense $Co_{0.67}Fe_{2.33}O_4$/YSZ monolith

little connectivity to the outer surfaces, probably because wall effects excluded the pore former from these regions during the extrusion process.

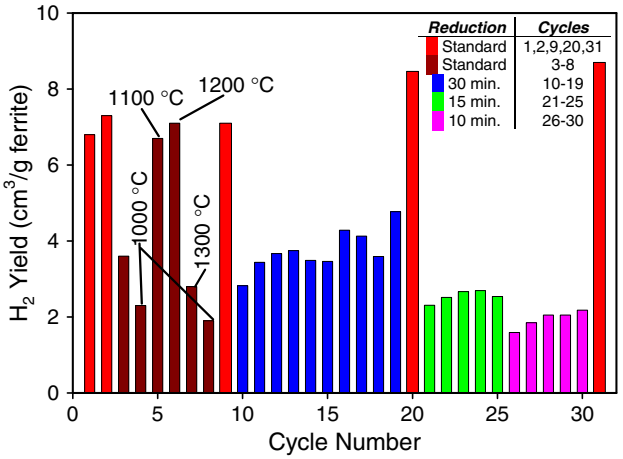

Fig. 10 Hydrogen yields for each water oxidation step carried out over a porous $Co_{0.67}Fe_{2.33}O_4$/YSZ monolith

Physical changes were evident in the porous sample after testing. The monolith shrunk during testing with of decrease of 18% in the diameter. Migration and coalescence of the small ferrite particles evidently occurred in parallel with the collapse of the porosity. The sample was uniformly black in color at the onset of the test, but it had taken on a "salt and pepper" appearance by the end of the evaluation with distinct black particles visible against a white or gray background. It is interesting that the apparent increase in ferrite particle size did not result in a decrease in H_2 yield.

On-sun testing of robocast monoliths (dense rods) similar to those described here has been conducted at the National Solar Thermal Test Facility (NSTTF) located at Sandia National Laboratories in Albuquerque, NM as the next logical step in preparing to test CR5 prototypes. In comparison to the laboratory reactor, the design of the solar reactor and the solar furnace allows the temperature and the gas environment sweeping the sample to be switched very rapidly (<1 min). The results at the NSTTF were consistent with laboratory testing; 3.5–4.0 cm^3 of H_2 were produced for each gram of ferrite in a $Co_{0.67}Fe_{2.33}O_4$/YSZ (1:4 by weight) monolith over several cycles (10 min TR at ~1,580 °C and 10 min WO and ~1,050 °C). These tests and facilities are described in greater detail elsewhere [25].

Ferrite utilization efficiency

In any test performed to date with a dense robocast monolith, the highest utilization efficiency achieved during a standard cycle was 22%. That is, the gas yield relative to the theoretical maximum gas yield (95 cm^3 H_2/g $Co_{0.67}Fe_{2.33}O_4$ at STP) was only 22%. It is straightforward to calculate a "penetration depth" of the reaction into the monolith rods from this number if one assumes that there is no geometric surface area lost where the rods overlap one another. If one

assumes an extent of reaction of 100%, i.e., that any portion of the ferrite that reacts fully reduces from $Co_{0.67}Fe_{2.33}O_4$ to CoO and FeO and back, then the reaction must penetrate 26 μm into the 450 μm rod to achieve 22% utilization. If more reasonable reaction extents of 50% or 25% are assumed, then the calculated penetration depths increase to 56 μm and 150 μm, respectively. For this monolith the average ferrite particle size prior to fabrication was 11 μm with 12 μm standard deviation.

The simple calculation shows that, even in the worst case, the sampling depth was greater than the average particle size, and suggests the intriguing possibility that interior particles (i.e., those without direct connectivity to the surface) in some way communicate with the surface and are available to react. A possible mechanism for this might involve transport of oxygen through vacancies in the YSZ phase. Alternate explanations include the possibility of gas transport through networks of micro-porosity or the formation of limited ferrite networks that connect to the surface (the ferrite loading is below the theoretical percolation limit). Additional experiments with variable rod sizes and particle sizes are planned to provide greater insight into this question.

The impact of ferrite loading on utilization was addressed by robocasting a series of dense $Co_{0.67}Fe_{2.33}O_4$/YSZ monoliths with ferrite:zirconia weight ratios of 1:10, 1:5, 1:4, 1:3, 1:2 , and 1:1.75. A 1:3 sample with 8% Y_2O_3 stabilized zirconia (as opposed to the standard 3%) was also fabricated. The $Co_{0.67}Fe_{2.33}O_4$ in each sample was all taken from the same large batch of material. The monoliths were each subjected to a mix of up to 11 standard cycles and alternate cycles. No patterns emerged in ferrite utilization efficiency; differences between the samples were generally within the range of cycle to cycle variability typically seen, with one exception. The sample with the highest ferrite loading (1:1.75 by weight) appeared to lose activity with cycling; the final standard cycle over this sample, the eleventh cycle overall, produced only half the H_2 of the first cycle. It may be significant that this material should be bi-continuous with the ferrite forming a percolating network rather than existing as isolated particles in a YSZ matrix. One would expect the positive support effect to diminish at high ferrite loadings, particularly once the ferrite particles can form a continuous phase.

Reaction rate considerations

Figure 11 shows O_2 and H_2 evolution as a function of time during the final standard cycle for the dense $Co_{0.67}Fe_{2.33}O_4$/YSZ monolith discussed in the section "Integration with CR5 design concept" (cycle 36, Fig. 9). Ideally, one would expect these curves to exhibit an initial high rate of reaction (gas evolution) associated with the surface and near surface and possibly a plateau at that rate if kinetics or

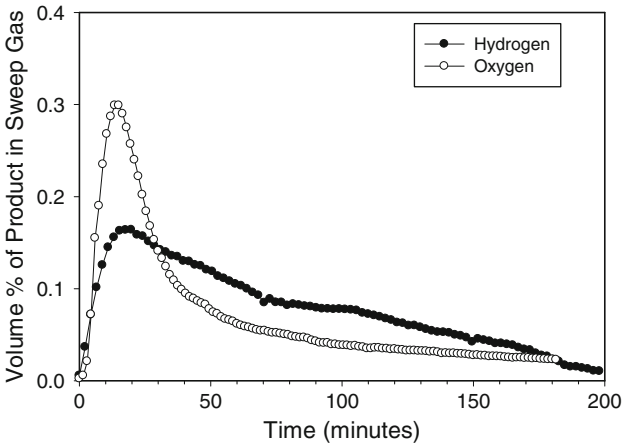

Fig. 11 Oxygen and hydrogen evolution from robocast $Co_{0.67}Fe_{2.33}O_4$/YSZ monolith with dense rods during cycle 36 (refer to Fig. 9)

mass transfer were slow relative to the number of these sites, and then a slow decline in reaction rate as bulk reaction and transport become necessary. In our case, the 10–15 min increase from no reaction to the maximum can be traced to the relatively high thermal mass of the furnace system coupled with gas dispersion resulting from relatively low flow rates in the large diameter reaction tube. Gas evolution curves in the solar furnace system resemble the ideal. It is clear from Fig. 11 that the reactions as practiced here are relatively slow, and that the initial stages of TR are more rapid than the initial stages of WO. The reasons for this are currently unknown, but surface reaction kinetics, thermodynamic driving forces, and mass transport to and away from the surface could all play a role. We are reasonably certain that transport within the bulk is not the rate limiting factor however as thermogravimetric analysis of the oxidation of thermally reduced samples with O_2 in air at 1,100 °C shows the reaction to be complete within several minutes.

The differences in reaction rate are not a particular concern for the CR5 design as they will eventually come to a balance under steady state operation. This point can be understood by examining Fig. 12, wherein the data from Fig. 11 is replotted so that rates are shown as a function of "total oxygen deficiency" in the monolith sample. The oxygen deficiency is defined as the integrated amount of O_2 evolved up to that point in time in the case of TR, or for WO the final O_2 deficiency at the end of the TR step minus ½ the amount of H_2 evolved and minus the total amount of O_2 the sample has been exposed to a result of background O_2 up to that point in time (plotted as Reoxidation, O_2 basis). Thus the TR step proceeds from left to right in Fig. 12, while WO (the back reaction) proceeds from right to left. A hypothetical unreacted packet of ferrite monolith

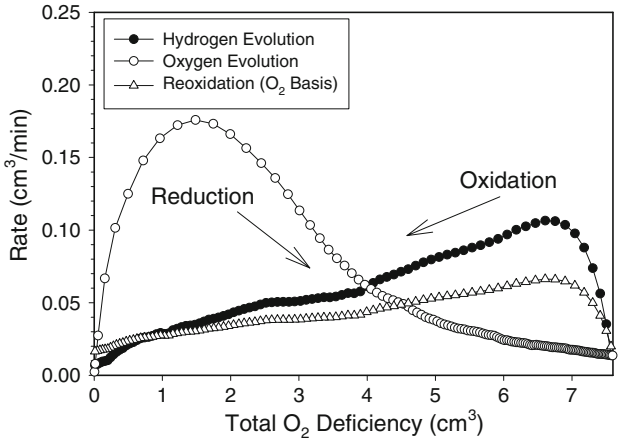

Fig. 12 Rates of O_2 evolution, H_2 evolution, and equivalent O_2 uptake during WO as a function of total oxygen deficiency in the monolith sample. Data adapted from Fig. 11

circling through the CR5 would first be reduced, represented in Fig. 12 as movement to the right on the O_2 evolution curve. Then, for a similar time period, it would be oxidized, represented by a drop to the reoxidation curve and a smaller movement back to the left (the rate is small as is the impact on oxygen deficiency). The packet would then again be thermally reduced and driven further along the WO curve to the right. The sequence would repeat until the sample is driven far enough into reduction that the rates of WO and TR converge and the process operates in the area where the TR and reoxidation curves cross one another.

In truth, the use of Fig. 12 for the above illustration is an oversimplification; the reason being that it is not simply the oxygen deficiency of the sample that determines the reaction rate, but the history of the sample as well. It is clear in the data from shorter cycles for example that if TR is interrupted after the evolution of only 4 cm^3 of O_2, then the initial H_2 evolution rate is significantly higher than that shown in Fig. 12 for an oxygen deficiency of 4 cm^3. If one assumes a simple shrinking core type model for the progress of both the TR and WO reactions in a rod geometry, it is clear that this should be expected. For this model, TR of a fully oxidized sample would result in an outer annular layer of reduced material. Subsequent WO would also proceed from the outside, resulting in cylinder of reduced material sandwiched between an inner core and outer eggshell of oxidized material. A similar volume of reduced material could be produced in a second sample as shallow surface layer by performing a shorter TR step. It is clear that the apparent reactivity of the surface layer and the inner ring would be different even though the total oxygen deficiencies of the two samples were identical.

In any case, what is important for CR5 operation is not the maximum rate of each reaction, but rather maximizing the kinetics of the reaction at the point where the two rates converge. This in fact may be a more important factor than how far one can drive a sample into and out of a reduced state, i.e., the maximum materials utilization. In other words it can be better to utilize a smaller percentage of material at a higher rate than a higher percentage at a smaller overall rate. This point may be further understood by reexamining the data in Figs. 9 and 10 in the context of Fig. 11. It is clear that when the TR time period is reduced, the H_2 yields do not suffer a proportional decrease. Thus a greater number of shorter cycles can result in larger overall yield than a single cycle carried out over the same time period.

Temperature is of course an important consideration for maximizing reaction rates. The limits of our laboratory furnace have effectively prevented us from addressing this issue for the TR step. Cycles 3–8 in Fig. 9 address the effect of temperature on the WO reaction. For these cycles, the TR step was performed as in the standard cycle. The WO step for cycles 4–8, however, was performed by decreasing the temperature to that shown and then initiating steam flow. For cycle 3, steam flow was initiated at 1,400 °C and the sample was allowed to cool to 900 °C. The results clearly show that the highest yields of H_2 were obtained at 1,100 and 1,200 °C. The poor yield at 1,300 °C is evidently the result of unfavorable thermodynamics. The poor yield at 900 and 1,000 °C is evidently the result of poor kinetics as the thermodynamics should be most favorable at the lowest temperatures.

The unfavorable thermodynamics for WO at 1,300 °C raises the possibility of using steam as an "inert" sweep gas that can easily be separated from O_2 produced during TR. Even if this were not done, it could alleviate concerns regarding crossover of steam from the WO side of the CR5 to the TR side. To evaluate this possibility, several cycles were performed with a porous robocast monolith utilizing the saturated Ar flow in place of the He sweep during the 1,400 °C TR step. The resulting H_2 yields during the WO steps were virtually indistinguishable from those with the He sweep in earlier and subsequent cycles. Nonetheless, longer-term evaluation of the effect of steam is required due to its tendency to degrade materials and enhance metal volatility [26].

Alternative chemistry

In our laboratories we have been interested in extending the basic thermochemical process approach to other useful chemistries and to other working materials. In particular we have applied the same approach to the carbon dioxide splitting (CDS) reaction ($CO_2 \rightarrow CO + ½\ O_2$) and to ceria-based oxides. Our interest in CDS is derived in part

from a comparison of the thermodynamics of CDS and WS. At temperatures above about 800 °C, CO_2 is less stable than H_2O, while at lower temperatures it is more stable. This is the consequence of a larger entropy term for the CDS reaction. The significance of this crossover is that for a given thermochemical system, the thermodynamics of CDS are more favorable than the thermodynamics of WS at any temperature >800 °C. However, if H_2 is the desired product, the water gas shift reaction is favorable at low temperature to produce H_2 from CO ($CO + H_2O \leftrightarrow H_2 + CO_2$). Additionally, CO is versatile in that syngas type chemistry can be used to produce hydrocarbon products, e.g., methanol ($CO + 2\ H_2 \rightarrow CH_3OH$).

A laboratory demonstration of thermochemical water splitting cycles based on the CeO_2/Ce_2O_3 pair was recently reported [27].

$$2CeO_2 \rightarrow Ce_2O_3 + {}^1/_2O_2$$

$$Ce_2O_3 + H_2O \rightarrow 2CeO_2 + H_2$$

Ceria is an active component in many catalysts and is known for its ability to store and release oxygen. For our purposes we were particularly cognizant of reports of Ce_2O_3 being directly oxidized by CO_2 to CeO_2, although a noble metal catalyst was also typically present [28–30]. Calculations indicate that CeO_2 spontaneously reduces (i.e., ΔG is negative) to Ce_2O_3 at temperatures above about 2,350 °C. Note that while below the reported melting point of CeO_2 (2,600 °C) this temperature is above the melting point of the product Ce_2O_3 (2,230 °C). In practice, partial reduction of ceria to various sub-oxides is possible at lower temperatures. A difficulty with ceria is that it is prone to sintering and that the oxygen storage and release is limited to the surface unless the material is modified with another oxide, typically zirconia. This modification also typically renders the material easier to reduce.

We have successfully performed CDS in our laboratories over our baseline $Co_{0.67}Fe_{2.33}O_4$/YSZ monoliths as well as monoliths cast from a $Ce_{0.25}Zr_{0.75}O_2$ material. Figure 13 compares WS and CDS (H_2 and CO evolution curves) over two nominally identical 1.6 g $Co_{0.67}Fe_{2.33}O_4$/YSZ robocasted monolithic lattice structures. In each case the material was thermally reduced at 1,400 °C in flowing inert gas for several hours. Following reduction, the temperature was lowered to 1,100 °C and then CO_2 (5% in He flowing at 55 sccm total) or water (50 sccm Ar saturated with steam at 80–90 °C) was fed over the monolith to produce CO or H_2 as shown in the figure. This sequence was repeated over seven cycles for the CDS case. Figure 13 shows that CDS over the ferrite is very similar to WS with an initial rapid conversion followed by a slow decline. The similarity suggests that similar processes are rate limited for both reactions. Despite the lower concentration of CO_2 in the reacting gas, yields are comparable, as is the general observation (which requires confirmation) that product yield increases with cycling (not shown here for WS).

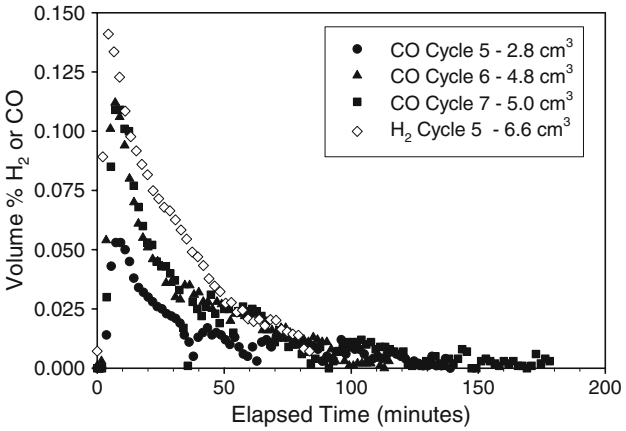

Fig. 13 Evolution of CO and H_2 over nominally identical robocast $Co_{0.67}Fe_{2.33}O_4$/YSZ monoliths with porous rods. Data for cycles 1–4 in the CDS case is not shown due to problems with O_2 leakage into the system. For WS, only cycle 5 (from Fig. 10) is shown for comparison to CDS; at this point the histories of each sample were similar. Total yields given in legend are normalized per gram of ferrite

Figure 14 illustrates WS and CDS over a ceria/zirconia composition. The material was co-precipitated with a nominal stoichiometry of $(CeO_2)_{0.25}(ZrO_2)_{0.75}$ from a solution of $Ce(NO_3)_3$ and $ZrOCl_2$ with NH_4OH, filtered, dried, calcined at 1,100 °C. Monoliths were cast from slurries of the finely ground product and pore former in a fashion similar to that previously described. The data in Fig. 14 was collected over a single 2.2 g, nominally 50% porous, disk. Four cycles of WS (cycle 3, typical of the others is shown) and a single cycle of CDS (with 10 and 20% CO_2 in He) were carried out over this composition. We attribute the greater yield of CO relative to H_2 over this material to decreased background O_2 levels when heat tracing is not required (as when CO_2 is fed). The slow increase, in CO concentration in the effluent over time, relative to WS, is an indication that the surface reaction rate is not only relatively slow, but that it also responds to the degree of reduction. That is, the WS data shows that this behavior does not result from dispersion in the flow system. The relatively slow decrease after the maximum is reached suggests that the rate of CDS in this regime is limited by surface processes. Both of these assertions are bolstered by the fact that the conversion responds rapidly to a doubling of the concentration of CO_2 in the feed stream. If true, the limited reaction rate of CO_2 over the ceria-based material likely results from the lack of a metal or metal ion capable of catalyzing C–O bond cleavage.

Other compositions with higher ceria content were also synthesized. In general, we observed that high ceria content

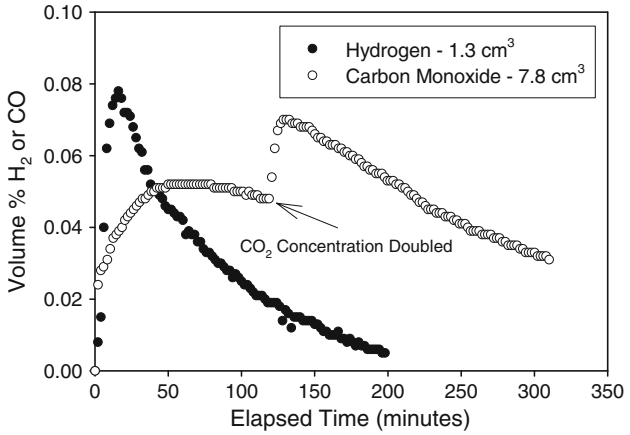

Fig. 14 Evolution of CO and H_2 over cast $Ce_{0.25}Zr_{0.75}$ monolith. Gas yields provided in legend are the total measured over the given cycle over the 2.2 g monolith

provided very high and thus more promising oxygen yields, but extensive sintering resulted in a total loss of porosity and subsequent reactivity. Monolithic structures comprised of large scale open networks may alleviate these problems. Nonetheless, Fig. 14 demonstrates, we believe for the first time, that both thermochemical WS and CDS proceed over ceria/zirconia at reasonable temperatures.

Summary

Two-step oxide-based thermochemical processes offer an exciting alternative to water electrolysis for H_2 production. However, in order for these processes to be truly competitive with electrolysis, energy management is essential. This fact makes efficient thermal recuperation between the high- and low-temperature reactions a virtual necessity. The CR5 is a new reactor concept that was designed to accomplish ferrite-based water splitting with thermal recuperation and simplicity of operation as guiding principles. As part of our efforts to develop a CR5 prototype, we have demonstrated that ferrite/zirconia mixtures may be directly fabricated into monolithic structures that are mechanically robust and that maintain productivity over at least tens of cycles with no apparent degradation in performance. Work is ongoing to maximize the utilization of the ferrite and the reaction rates of the monoliths. Our baseline choice of material for the prototype is a mixture of $Co_{0.67}Fe_{2.33}O_4$ and YSZ in a 1:3 weight ratio. Future work will consider Ni-substituted materials ($NiFe_2O_4$) that are indicated as the optimum material by thermodynamics.

Many questions remain unanswered regarding the basic processes taking place during both the TR and WO steps. Additionally, the role of "inert" supports such as YSZ in stabilizing ferrites over multiple water splitting cycles is not well understood as both physical (particle isolation) and chemical (Fe dissolution, oxygen transport) mechanisms may contribute. CDS is a thermodynamically favorable alternative to water splitting that can be used to produce H_2 or even hydrocarbons. We have demonstrated thermochemical CDS, we believe for the first time, over both ferrite and ceria-base monoliths and believe that this approach merits much greater consideration.

Acknowledgement Sandia is a multiprogram laboratory operated by Sandia Corporation, a Lockheed Martin Company, for the United States Department of Energy's National Nuclear Security Administration under Contract DE-AC04-94AL85000.

References

1. Lewis NS, Nocera DG (2006) Proc Natl Acad Sci USA 103:15729
2. Dukes JS (2003) Clim Change 61:31
3. Ivy J (2004) Summary of electrolytic hydrogen production. National Renewable Energy Laboratory report NREL/MP-560-36734
4. Abanades S, Charvin P, Flamant G, Neveu P (2006) Energy 31:2469
5. Funk JE, Reinstrom RM (1966) Ind Eng Chem Process Des Develop 5:336; Abraham BA, Schreiner F (1974) Ind Eng Chem Fund 13:305
6. Nakamura T (1977) Sol Energy 19:467
7. Kodama T, Kondoh Y, Kiyama A, Shimizu K (2003) In: Thornbloom MD, Jones SA, (eds) Proceedings of the ASME international solar energy conference (ISEC), ASME, Hawaii, p 121
8. Ehrensberger K, Kuhn P, Shklover V, Oswald HR (1996) Solid State Ionics 90:75
9. Ehrensberger K, Frei A, Kuhn P, Oswald HR, Hug P (1995) Solid State Ionics 78:151
10. Tamaura Y, Steinfeld A, Kuhn P, Ehrensberger K (1995) Energy 20:325
11. Tamaura Y, Kojima M, Sano T, Ueda Y, Hasegawa N, Tsuji M (1998) Int J Hydrogen Energy 23:1185
12. Ishihara H, Kaneko H, Yokoyama T, Fuse A, Tamaura Y (2006) In: Proceedings of the 2005 international solar energy conference (ISEC), ASME, Orlando, FL, 2005, p 687
13. Aoki H, Kaneko H, Hasegawa N, Ishihara H, Takahashi Y, Suzuki A, Tamaura Y (2004) In Proceedings of 2004 international solar energy conference (ISEC), ASME, Portland, OR, p 515
14. Kodama T, Kondoh Y, Yamamoto R, Andou H, Satou N (2005) Sol Energy 78:623
15. Diver RB, Miller JE, Allendorf MD, Siegel NP, Hogan RE (2006) In: Proceedings of the 2006 international solar energy conference (ISEC), ASME, Denver, CO
16. Miller JE, Evans LR, Stuecker JN, Allendorf MD, Siegel NP, Diver RB (2006) In: Proceedings of the 2006 international solar energy conference (ISEC), ASME, Denver, CO
17. James DL, Siegel NP, Diver RB, Boughton BD, Hogan RE (2006) In: Proceedings of the 2006 international solar energy conference (ISEC), ASME, Denver, CO
18. Allendorf MD, Miller JE, Siegel NP, Diver RB (2006) In: Proceedings of the 2006 international solar energy conference (ISEC), ASME, Denver, CO
19. Erickson DS, Mason TO (1985) J Solid State Chem 59:42
20. Allendorf MD, Miller JE, Siegel NP, Diver RB, Energy Fuel (submitted)
21. Roeb M, Sattler C, Kluser R, Monnerie L, Konstandopoulos AG, Agrafiotis C, Zaspalis VT, Nalbandian L, Steele A, Stobbe P

(2006) In: Proceedings of the 2005 international solar energy conference (ISEC), ASME, Orlando, FL, 2005, p 671
22. Stuecker JN, Miller JE, Ferrizz RE, Mudd JE, Cesarano J III (2004) Ind Eng Chem Res 43:51
23. Stuecker JN, Cesarano J III, Hirschfeld DA (2003) J Mater Process Technol 142:318; Cesarano J III, Calvert PD (2000) U.S. Patent 6,027,326; Cesarano J III, Segalman R, Calvert P (1998) Ceramic Ind 148:94
24. Ferrizz RM, Stuecker JN, Cesarano J III, Miller JE (2005) Ind Eng Chem Res 44:302
25. Diver RB, Siegel NP, Miller JE, Moss TA, Stuecker JN, James DL (2008) In: Proceedings of 2008 14th Biennial CSP solar PACES symposium, Las Vegas, NV
26. McCarty JG, Gusman M, Lowe DM, Hildenbrand DL, Lau KN (1999) Catal Today 47:5
27. Abanades S, Flamant G (2006) Sol Energy 80:1611
28. Sharma S, Hilaire S, Vohs JM, Gorte RJ, Jen H-W (2000) J Catal 190:199
29. Bernal S, Blanco G, Gatica JM, Larese C, Vidal H (2001) J Catal 200:411
30. Demoulin O, Navez BM, Mugabo JL, Ruiz P (2007) Appl Catal B 70:284